Acta Crystallographica Section D
Biological Crystallography
ISSN 0907-4449

Structures of free and inhibited forms of the L,D-transpeptidase Ldt_{Mt1} from *Mycobacterium tuberculosis*

Stefania Correale,[a,b]‡ Alessia Ruggiero,[a]‡ Rosanna Capparelli,[c] Emilia Pedone[a] and Rita Berisio[a]*

[a]Institute of Biostructures and Bioimaging, CNR, Via Mezzocannone 16, 80134 Napoli, Italy, [b]Kedrion S.p.A, 80029 S. Antimo (Napoli), Italy, and [c]Department of Soil, Plant, Environmental and Animal Production Sciences, School of Biotechnological Sciences, University of Naples 'Federico II', Portici, Italy

‡ These authors contributed equally to this work.

Correspondence e-mail: rita.berisio@unina.it

Received 15 March 2013
Accepted 13 May 2013

PDB References: Ldt_{Mt1}, 4jmn; complex with imipenem, 4jmx

The modelling of peptidoglycan is responsible for key cellular processes in *Mycobacterium tuberculosis* such as cell growth, division and resuscitation from dormancy. The structure of *M. tuberculosis* peptidoglycan is atypical since it contains a majority of 3,3 cross-links synthesized by L,D-transpeptidases that replace the 4,3 cross-links formed by the D,D-transpeptidase activity of classical penicillin-binding proteins. Carbapenems inactivate these L,D-transpeptidases and in combination with clavulanic acid are bactericidal against extensively drug-resistant *M. tuberculosis*. Here, crystal structures of the L,D-transpeptidase Ldt_{Mt1} from *M. tuberculosis* in a ligand-free form and in complex with the carbapenem imipenem are reported. Elucidation of the structural features of Ldt_{Mt1} unveils analogies and differences between the two key transpeptidases of *M. tuberculosis*: Ldt_{Mt1} and Ldt_{Mt2}. In addition, the structure of imipenem-inactivated Ldt_{Mt1} provides a detailed structural view of the interactions between a carbapenem drug and Ldt_{Mt1}. By providing the key interactions in the binding of carbapenem to Ldt_{Mt1}, this work will facilitate structure-guided discovery of L,D-transpeptidase inhibitors as novel antitubercular agents against drug-resistant *M. tuberculosis*.

1. Introduction

Tuberculosis (TB) is a global emergency that is not restricted to developing countries, as declared by the Horizon 2020 Plan and by the World Health Organization Global Plan to Stop TB 2011–2015. The continuous emergence of resistance to currently adopted drugs, which first developed 40 years ago, is a major threat to the control of this disease, with all countries being at risk. Therefore, the development of new drugs with novel mechanisms of action is an urgent necessity (Murillo *et al.*, 2007; Chim *et al.*, 2011). *Mycobacterium tuberculosis* (Mtb) is the aetiologic agent of TB and shares a unique cell wall with other members of the *Mycobacterium* genus which plays a key role in the development of drug resistance and in bacterial survival under stress conditions (Trefzer *et al.*, 2012). This cell wall is composed of three main layers: a highly impermeable layer of mycolic acids, a polysaccharide called arabinogalactan and a peptidoglycan (PGN) layer attached to the cytoplasmatic membrane. PGN is a polymer formed by glycan chains of β-(1–4)-linked-*N*-acetylglucosamine (GlcNAc) and *N*-acetylmuramic acid (MurNAc) cross-linked by short peptide stems. PGN of *M. tuberculosis* is classified as *meso*-diaminopimelic acid (DAP)-type since it includes a DAP residue at the third position of the peptide stem. The modelling of PGN is responsible for key cellular processes of Mtb such as cell growth and division, and resuscitation from dormancy, a metabolically inactive state that allows the bacteria to survive

adverse physical-chemical conditions or nutrient starvation (Ruggiero *et al.*, 2009, 2010, 2011, 2012, 2013; Mukamolova, Yanopolskaya *et al.*, 1998; Mukamolova, Kaprelyants *et al.*, 1998; Squeglia *et al.*, 2011; Dworkin & Shah, 2010; Kaprelyants *et al.*, 2012). This bacterial dormant state is responsible for a latent infection affecting one third of the world's population. However, the precise nature of the Mtb cells associated with latent tuberculosis is presently not clear.

The peptidoglycan structure of Mtb from a stationary-phase culture revealed a high content (80%) of nonclassical 3,3 cross-links generated by L,D-transpeptidation (Lavollay *et al.*, 2008), whereas the classical 4,3 cross-links are predominantly formed by the D,D-transpeptidase activity of penicillin-binding proteins (PBPs) during the exponential phase of growth (Dubée, Triboulet *et al.*, 2012; Gupta *et al.*, 2010; Lecoq *et al.*, 2012). L,D-Transpeptidases and PBPs are structurally unrelated and contain active-site cysteine and serine residues, respectively. L,D-Transpeptidases were first identified in an ampicillin-resistant mutant of *Enterococcus faecium* and were associated with a bypass mechanism of the D,D-transpeptidases involved in PGN synthesis (Mainardi *et al.*, 2005). This mechanism involves the transfer of the peptide bond from the third residue (L chiral centre) of a tetrapeptide donor stem to the side-chain amide group of the third residue (D chiral centre) of an adjacent acceptor stem. Catalysis proceeds by a two-step mechanism: (i) production of PGN precursors devoid of the C-terminal residue D-Ala5 (by a DD-carboxypeptidase), which are substrates of L,D-transpeptidases, and (ii) catalysis by L,D-transpeptidases of the formation of 3,3 cross-links instead of the 4,3 cross-links formed by the D,D-transpeptidases of the classical PBP family (Dubée, Triboulet *et al.*, 2012; Gupta *et al.*, 2010; Lecoq *et al.*, 2012; Fig. 1).

Among the five paralogues of L,D-transpeptidase in Mtb, Ldt_{Mt1} and Ldt_{Mt2} have been shown to be functional in an *in vitro* peptidoglycan cross-linking assay (Gupta *et al.*, 2010; Dubée, Triboulet *et al.*, 2012). Ldt_{Mt2} is essential for virulence in a mouse model of acute infection (Gupta *et al.*, 2010), whereas Ldt_{Mt1} is thought to play a critical role in peptidoglycan adaptation to the nonreplicative state of the bacillus (Lavollay *et al.*, 2008). Both Ldt_{Mt1} and Ldt_{Mt2} have been shown to be inactivated by carbapenems, a class of β-lactam antibiotics (Dubée, Triboulet *et al.*, 2012; Lecoq *et al.*, 2012; Dubée, Arthur *et al.*, 2012; Lavollay *et al.*, 2008; Mainardi *et al.*, 2007). This class of antibiotics have long been considered to be inadequate for the treatment of tuberculosis because Mtb produces BlaC, an extended-spectrum class A β-lactamase (Hugonnet & Blanchard, 2007). However, the finding that BlaC is irreversibly inactivated by clavulanic acid (Hugonnet & Blanchard, 2007) has prompted the use of β-lactams in combination with clavulanic acid. Combined with clavulanic acid, carbapenems (in particular imipenem and meropenem) significantly reduced the bacterial burden in Mtb-infected macrophages (England *et al.*, 2012), and meropenem has been reported to show *in vitro* bactericidal activity against extensively drug-resistant Mtb (XDR-TB; Hugonnet *et al.*, 2009). Therefore, the development of L,D-transpeptidase inhibitors belonging to the β-lactam family is a novel and promising approach to obtain drugs for the treatment of XDR-TB.

Despite the key role of L,D-transpeptidation enzymes in Mtb, structural information on these enzymes has only recently emerged. After we had solved the structure of Ldt_{Mt1} (Correale *et al.*, 2013), several descriptions of the structure of Mtb Ldt_{Mt2} were reported (Böth *et al.*, 2013; Kim *et al.*, 2013; Erdemli *et al.*, 2012), whereas no structural data are available to date for Ldt_{Mt1}. In this study, we investigate the structural features of Mtb Ldt_{Mt1} in both a ligand-free form and in complex with the carbapenem imipenem by combining X-ray crystallography, spectroscopic and calorimetric assays. The crystal structure of Ldt_{Mt1} shows that the catalytic site is located in a tiny tunnel, a finding that suggests a high specificity of Ldt_{Mt1} for its substrates, as was observed for the L,D-transpeptidase from *E. faecium* (Magnet *et al.*, 2007). In addition to a detailed molecular picture of Ldt_{Mt1}, this study yields new structural insights into the irreversible inhibition of Ldt_{Mt1} by the carbapenem imipenem. Together with the recently determined structures of Ldt_{Mt2} (Böth *et al.*, 2013; Kim *et al.*, 2013; Erdemli *et al.*, 2012), this study completes the structural description of L,D-transpeptidation enzymes in Mtb and opens up to further expansion the development of L,D-transpeptidase inhibitors belonging to the β-lactam family for the treatment of extensively drug-resistant TB.

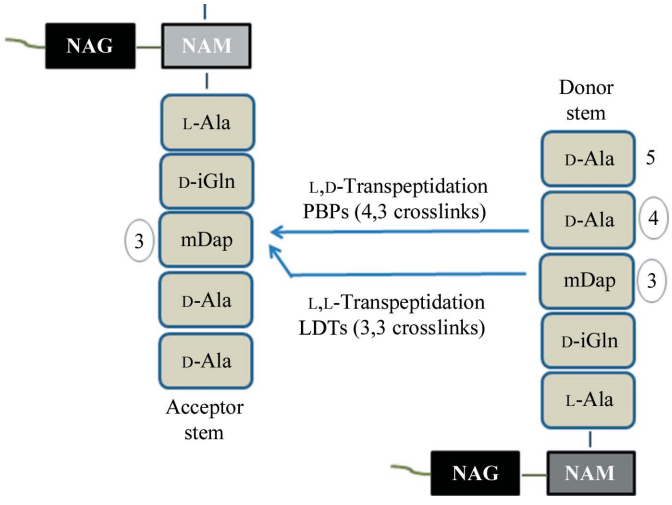

Figure 1
Schematic representation of peptidoglycan transpeptidation. L,D-Transpeptidases catalyse the formation of the bond between the carbonyl of mDap3 of the donor strand and the side chain of mDap3 of the acceptor stem (3,3 cross-link).

2. Experimental procedures

2.1. Sequence-conservation studies

Sequence-conservation studies were carried out using *ConSurf* (Goldenberg *et al.*, 2009). The homologue-search algorithm *CSI-BLAST* was used to retrieve sequences from the UNIREF-90 sequence database using an *E*-value cutoff of 0.001 (150 sequences). Sequences were aligned using the *MAFFT* L-INS-i alignment method.

2.2. Production and purification of recombinant proteins

Ldt_{Mt1} (residues 32–251) was initially cloned and expressed as reported by Correale *et al.* (2013). However, although the crystallographic data allowed us to determine the phases, refinement led to high values of the *R* factor and R_{free} owing to twinning of the crystals. Therefore, we recloned the protein by introducing a C-terminal hexahistidine tag using the pETM-13 vector. Protein expression was achieved using *Escherichia coli* BL21(DE3) harbouring the pREP4/GroESL plasmid after overnight induction in 0.5 m*M* IPTG at 289 K. The protein was purified from clarified lysate by affinity chromatography on a 5 ml Ni–NTA (Ni^{2+}–nitrilotriacetate) column (GE Healthcare). An additional size-exclusion chromatography step was performed on a Superdex HR 10/30 column (GE Healthcare) equilibrated in 50 m*M* Tris–HCl pH 7.8, 150 m*M* NaCl, 5%(*v*/*v*) glycerol, 0.01%(*w*/*v*) CHAPS at a flow rate of 0.5 ml min^{-1}. The protein was concentrated by ultrafiltration (Amicon Ultra-4 centrifugal filter devices, Millipore) and the concentration was determined using the Bradford protein assay (Bio-Rad Laboratories). Fresh concentrated protein at 5 mg ml^{-1} was used for crystallization experiments. A selenomethionine derivative of Ldt_{Mt1} ($SeMetLdt_{Mt1}$) was prepared and was purified as described above.

2.3. Crystallization, data collection and processing

Crystallization trials were performed using the hanging-drop vapour-diffusion method. Crystals of native Ldt_{Mt1} were obtained using a protein concentration of 3.5 mg ml^{-1} with 1.24 *M* sodium phosphate, 0.16 *M* potassium phosphate, 10 m*M* TCEP pH 5.6. The conditions were optimized for the crystallization of SeMet-derivatized Ldt_{Mt1}. A pre-incubation of the crystallization trials at 277 K was performed to induce nucleation. Once small needles were detectable, the crystallization plates were gradually brought to 293 K. This temperature increase led to better growth of crystals, which reached dimensions of 0.02 × 0.02 × 0.8 mm. MAD data were collected from a cryocooled SeMet-derivative crystal (100 K) on beamline BM14 at the ESRF, Grenoble, France at wavelengths determined from the selenium absorption spectrum (Table 1). Crystals of the complex between Ldt_{Mt1} and imipenem were obtained after overnight soaking of native crystals in an 8 m*M* imipenem solution. Cryoprotection of the crystals was achieved by a fast soaking in a solution containing glycerol at a final concentration of 25%(*v*/*v*). The data sets were scaled and merged using the *HKL*-2000 package (Otwinowski & Minor, 1997). Data-collection statistics are reported in Table 1.

2.4. Structure determination and refinement

SOLVE (Terwilliger, 2004) was used to localize the selenium sites present in the asymmetric unit and to derive the experimental phases. The phases were improved by density modification using *RESOLVE* (Terwilliger, 2004) and *ARP*/*wARP* (Langer *et al.*, 2008). Crystallographic refinement was first carried out against 95% of the measured data using the *CCP*4 suite (Winn *et al.*, 2011). The remaining 5% of the observed data, which were randomly selected, were used in R_{free} calculations to monitor the progress of the refinement. The structure was validated using *PROCHECK* (Laskowski *et al.*, 1996).

Table 1
Data-collection and refinement statistics.

Values in parentheses are for the highest resolution shell.

	Peak	Remote	Imipenem complex
Data collection			
Space group	$P4_32_12$	$P4_32_12$	$P4_32_12$
Unit-cell parameters (Å)	$a = b = 67.25$, $c = 119.75$	$a = b = 67.42$, $c = 119.97$	$a = b = 67.40$, $c = 119.56$
Resolution range (Å)	50.00–2.24 (2.28–2.24)	50.00–2.20 (2.24–2.20)	50.00–2.55 (2.59–2.55)
Wavelength (Å)	0.978	0.954	0.978
Mosaicity (°)	0.20	0.20	0.75
Average multiplicity	15.6 (15.7)	13.6 (15.0)	8.9 (8.7)
Unique reflections	14625	14669	9506
Completeness (%)	100.0 (100.0)	100.0 (100.0)	99.8 (99.8)
R_{merge}† (%)	8.4 (43.8)	9.0 (42.8)	9.0 (43.2)
Average $I/\sigma(I)$	18.1 (5.3)	13.1 (5.7)	14.1 (2.6)
Refinement			
R_{work}/R_{free} (%)	16.7/21.3		17.2/22.4
No. of residues	216		216
No. of water molecules	300		280
R.m.s. deviations			
Bond lengths (Å)	0.009		0.009
Bond angles (°)	1.5		1.4

† $R_{merge} = \sum_{hkl}\sum_i |I_i(hkl) - \langle I(hkl)\rangle| / \sum_{hkl}\sum_i I_i(hkl)$, where $I_i(hkl)$ is the intensity of the *i*th measurement of reflection *hkl* and $\langle I(hkl)\rangle$ is the mean value of the intensity of reflection *hkl*.

2.5. Circular dichroism

To analyze the conformational state of Ldt_{Mt1}, far-UV CD spectra were measured at 293 K. All CD spectra were recorded with a Jasco J-810 spectropolarimeter equipped with a Peltier temperature-control system (Model PTC-423-S). Molar ellipticity per mean residue, $[\theta]$, in deg cm^2 $dmol^{-1}$ was calculated from the equation $[\theta] = [\theta]_{obs} \times mrw \times (10lC)^{-1}$, where $[\theta]_{obs}$ is the ellipticity measured in degrees, mrw is the mean residue molecular mass (108.2 Da), *C* is the protein concentration in g l^{-1} and *l* is the optical path length of the cell in centimetres. Far-UV measurements (195–250 nm) were carried out at 293 K using a 0.1 cm optical path-length cell and a protein concentration of 0.2 mg ml^{-1}.

2.6. Isothermal titration calorimetry

Thermodynamic parameters characterizing the interaction of Ldt_{Mt1} with imipenem were determined by isothermal titration calorimetry (ITC). These experiments were carried out using a 50 μ*M* concentration of Ldt_{Mt1} and a 1:8 protein: inhibitor molar ratio in 100 m*M* sodium phosphate buffer pH 6.0. The exothermic heat peaks exhibited a monotonic decrease with the addition of the ligand until saturation was reached. The data could best be fitted using a nonlinear least-squares approach to the 'one-set-of-sites' binding model.

3. Results and discussion

3.1. Overall structure of Ldt_{Mt1}

Analysis of the sequence of the L,D-transpeptidase Ldt_{Mt1} predicts the existence of a transmembrane helix at the protein N-terminus (residues 7–29), a finding which suggests that Ldt_{Mt1} is bound to the bacterial cytoplasmatic membrane. An analysis of the PFAM database (Finn *et al.*, 2006) clearly identifies (*E*-value 2.9 × 10^{-20}) the L,D-transpeptidase catalytic domain as the C-terminal domain (residues 125–249; Ykud family, PF03734). This domain is preceded by a further domain whose structure cannot unambiguously be predicted based on its sequence (Fig. 2*a*). Based on sequence analysis, we have cloned and expressed Ldt_{Mt1} deprived of its transmembrane helix. The recombinant Ldt_{Mt1} was found to be monomeric in solution, as shown by both size-exclusion chromatography and light scattering (data not shown). Circular-dichroism spectra indicate a good degree of structural integrity of the protein (Supplementary Fig. S1[1]). Crystals of Ldt_{Mt1} that were suitable for X-ray studies were obtained using vapour-diffusion techniques and belonged to the tetrahedral space group $P4_32_12$. The structure was solved using the multiple anomalous dispersion (MAD) method and was refined at 2.2 Å resolution. For details of data processing, refinement and structure validation, see Table 1.

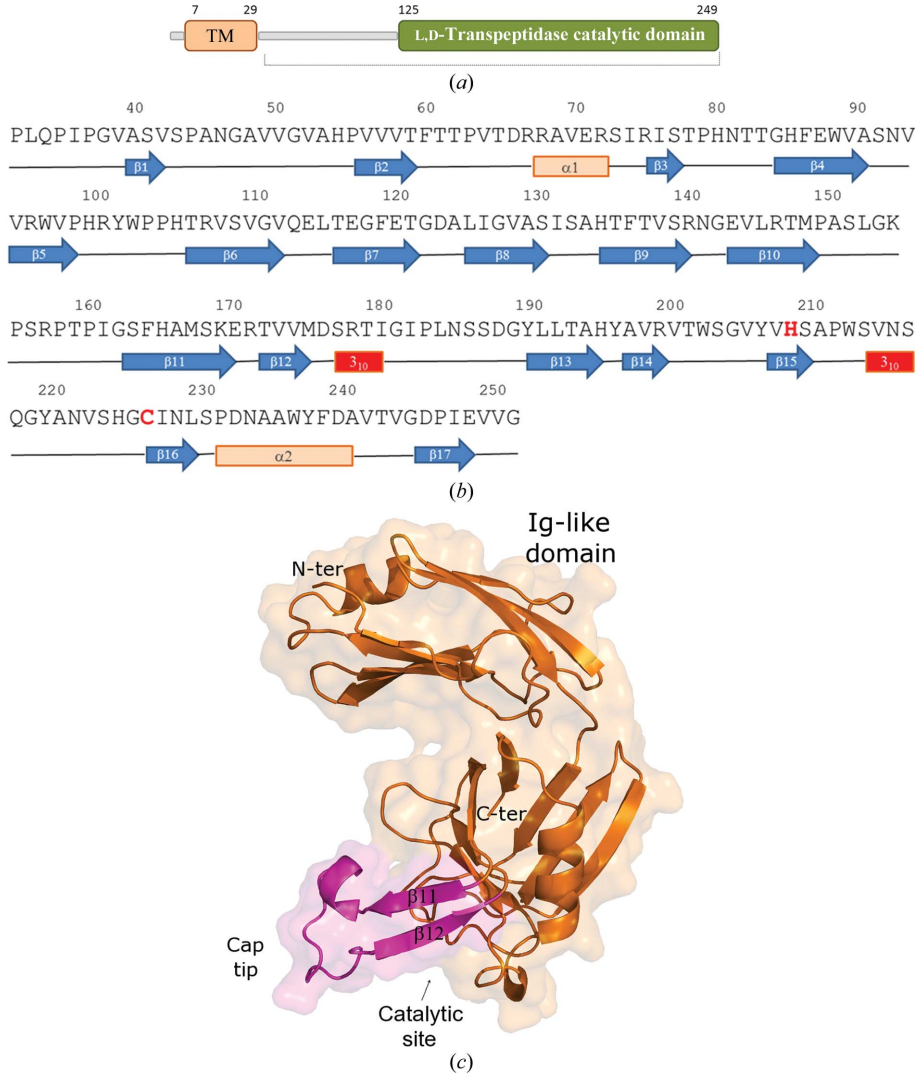

Figure 2
Structural features of Ldt_{Mt1}. (*a*) Domain organization of Ldt_{Mt1} according to the PFAM database (Finn *et al.*, 2006). (*b*) Secondary-structure elements of Ldt_{Mt1} based on its crystal structure. (*c*) Cartoon and surface representation of the overall shape of the Ldt_{Mt1} structure. The insert covering the catalytic domain is shown in orange.

The overall crystal structure of Ldt_{Mt1} exhibits a semicircular shape formed by two domains connected by a short loop (residues 121–125; Figs. 2*b* and 2*c*). A large number of hydrogen bonds exist between the two domains and/or involve the connecting loop, some of which occur through backbone atoms (between the loop 242–248 and the N-terminal part of β-strand β17; residues 243–245). This feature suggests that the bent shape of the molecule may be instrumental to its function. The N-terminal domain of Ldt_{Mt1} (residues 32–122) resembles a c-type immunoglobulin (Ig) domain (Berisio *et al.*, 2012) composed of two four-stranded β-sheets packed against each other and an α-helix (α1 in Fig. 2*c*). Notably, most structurally related Ig domains identified using the *DALI* server show extremely poor sequence identity to the Ldt_{Mt1} Ig-like domain, ranging between 5 and 11% (Supplementary Table S1), an observation which explains the difficulty of fold-prediction software in classifying this domain as Ig-like (Fig. 2*a*). The structure of the Ldt_{Mt1} catalytic domain consists of a β-sandwich with two mixed sheets, which form a cradle capped by an α-helix (Fig. 2*c*).

3.2. Ldt_{Mt1} catalytic centre

Electron-density maps provide a detailed picture of the Ldt_{Mt1} catalytic site and allow unambiguous identification of the conformation of the enzyme catalytic residues (Fig. 3). Cys226 is located at the N-terminus of β-strand β16 and faces the conserved His208 belonging to the β-strand β15 (Fig. 3*b*). Typically, the third catalytic residue of cysteine proteases plays the role of keeping histidine in the correct conformation and tautomeric form for the catalytic reaction (Lecoq *et al.*, 2012; Ruggiero *et al.*, 2010). In the crystal structure of Ldt_{Mt1}, His208 is hydrogen-bonded to the backbone carbonyl O atom of

[1] Supplementary material has been deposited in the IUCr electronic archive (Reference: DZ5284). Services for accessing this material are described at the back of the journal.

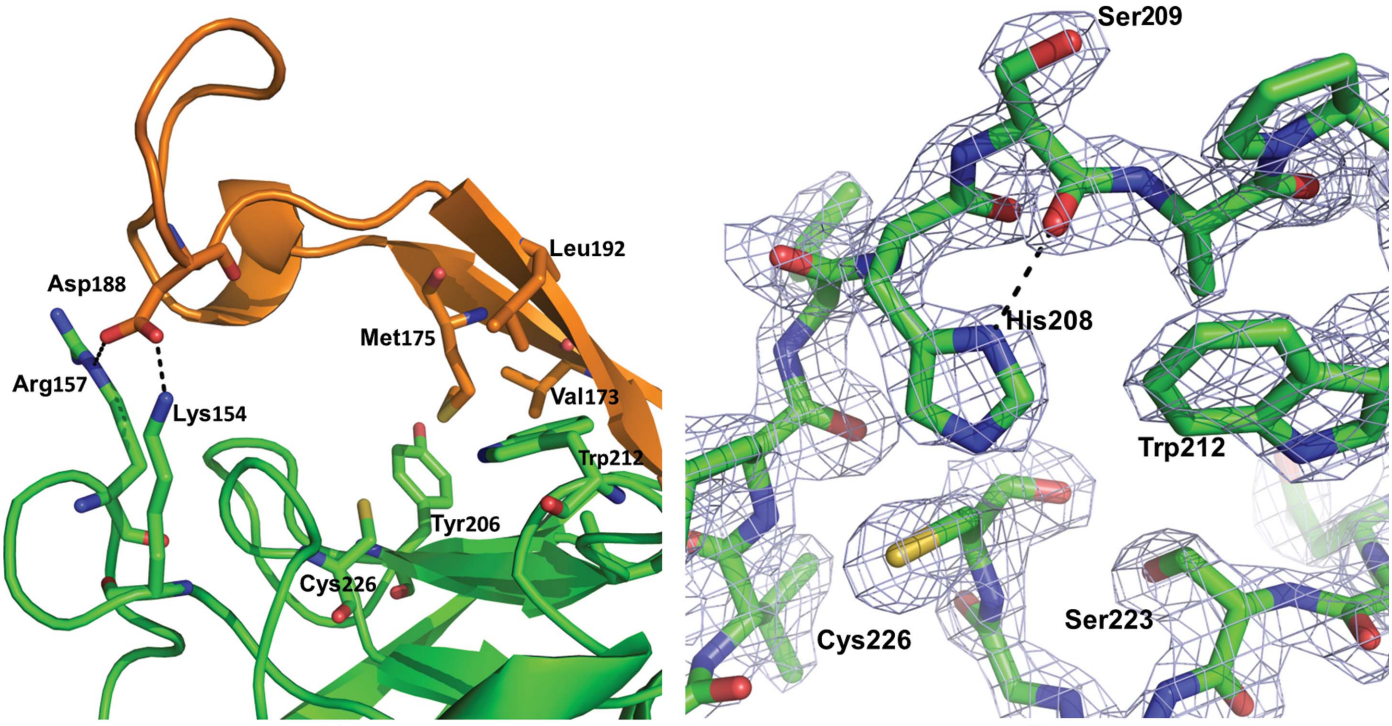

Figure 3
Details of the Ldt_{Mt1} structure. (*a*) The Ldt_{Mt1} pincer. Hydrophobic/aromatic residues involved in interactions of the two-stranded β-sheet of the cap and residues involved in salt-bridge formation are shown in stick representation. Cys226 is also shown for identification of the catalytic pocket. (*b*) $(2F_o - F_c)$ electron-density map of the Ldt_{Mt1} catalytic site contoured at 2.0σ.

Ser209 (Fig. 3*c*). This interaction identifies Ser209 as the third catalytic residue. An analysis of the sequence conservation of the protein, carried out with *ConSurf* (Goldenberg *et al.*, 2009), clearly shows that the predicted catalytic residues Cys226 and His208 are fully conserved, whereas the third residue of the catalytic triad is not clearly identifiable (Supplementary Figs. S2 and S3). The fact that hydrogen bonding to His208 is mediated by the backbone of Ser209 explains why this latter residue is not conserved.

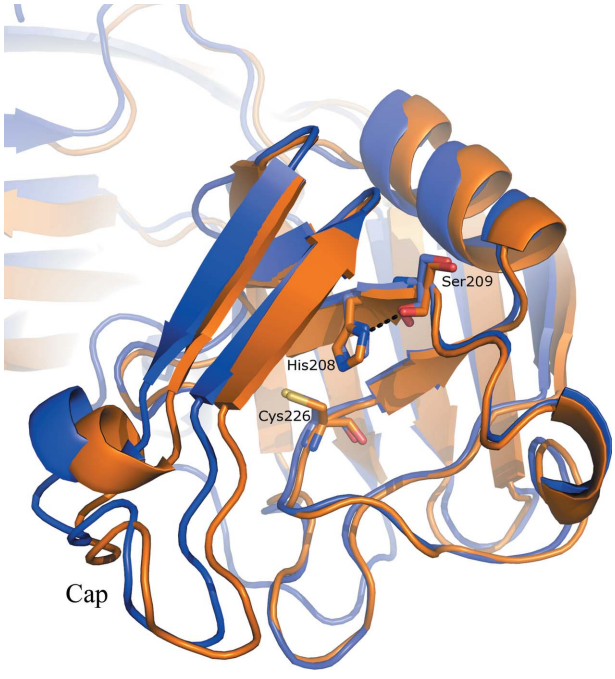

Figure 4
Superposition of the catalytic domain of Ldt_{Mt1} (orange) on that of Ldt_{Mt2} (PDB entry 3u1q; slate blue). Catalytic residues are drawn in stick representation.

Based on the crystal structure of Ldt_{Mt1}, we computed the pK_a values of the catalytic residues using *PROPKA* (Rostkowski *et al.*, 2011). This analysis produces a pK_a value of 11.1 for Cys226, whereas the pK_a of His208 is downshifted to 4.6, likely owing to the highly hydrophobic environment of this residue. These pK_a values suggest that Cys226 remains protonated at neutral pH, whereas His208 is positively charged. Therefore, Ldt_{Mt1} acts through a hydrogen-bonded thiol–imidazole pair (SH/N) for catalysis, which differs from the thiolate–imidazolium (S^-/NH^+) ion pair typically found in papain-like proteases, the catalytic cysteines of which exhibit anomalously low pK_a values (Gul *et al.*, 2008). Therefore, His208 is likely to play the role of activating Cys226 by acting as a general base for nucleophilic attack during the transpeptidase reaction.

In accordance with the recently determined structures of Ldt_{Mt2} (Böth *et al.*, 2013; Kim *et al.*, 2013; Erdemli *et al.*, 2012), the active site of Ldt_{Mt1} is located under a lid formed by a long insert between β-strands $\beta11$ and $\beta14$ consisting of a two-stranded β-sheet, a short 3_{10}-helix and a long loop (Fig. 2*c*). This lid covering the catalytic site does not exist in the L,D-transpeptidase from *B. subtilis* and is disordered in the structure of the L,D-transpeptidase from *E. faecium* (Biarrotte-

Sorin *et al.*, 2006). Analysis of the crystal structure shows that the two-stranded β-sheet region of the insert, here denoted the 'cap', is tightly bound to the β-sandwich through hydrophobic interactions involving residues that are all well conserved (Figs. 3*a* and 4). Conversely, only a few interactions involve the cap tip in a pincer-like fashion: namely, a salt bridge involving Asp188 and the two positively charged residues Lys154 and Arg157 belonging to the facing loop (Fig. 3*a*). Since the cap does not completely cover the catalytic site of Ldt_{Mt1} but leaves it partially solvent-accessible, the question remains as to whether the cap is locked during enzyme catalysis or whether it opens up to host the substrate. The existence of only a few interactions involving the cap tip suggests that open and closed conformations of the cap exist in solution and that the closed conformation locks the bound state. This hypothesis is corroborated by the finding that the cap tip is disordered in the crystal structure of the apo form of Ldt_{Mt2} (Kim *et al.*, 2013) and in the available structures of the L,D-transpeptidase of *E. faecium* (PDB entries 1zat and 2hkl).

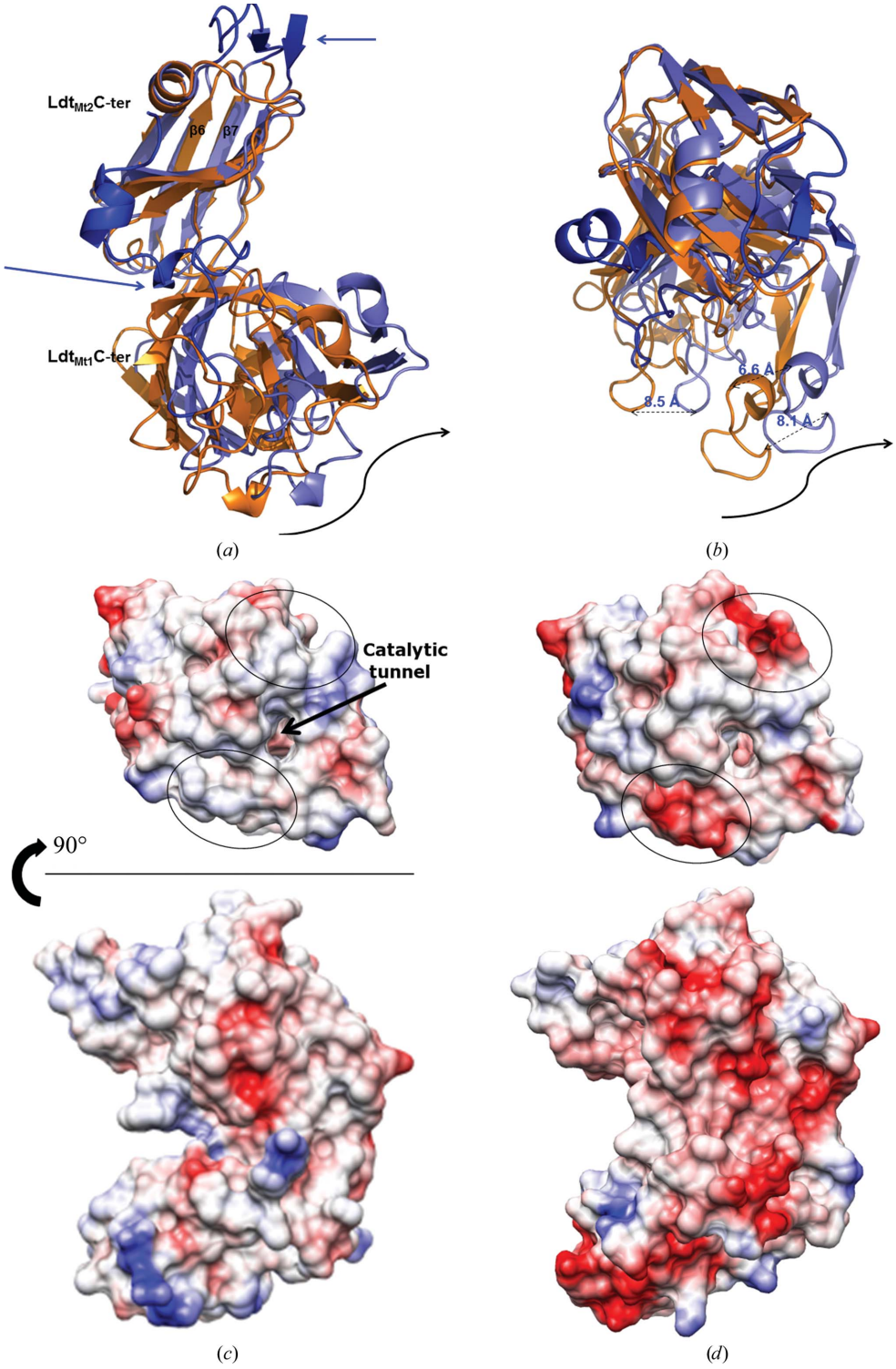

Figure 5
Superposition of Ldt_{Mt1} (orange) on the Ldt_{Mt2} structure (PDB entry 3u1q; slate blue). (*a*, *b*) Side and top views after superposition of the Ig-like domains. Insertions in Ldt_{Mt2} are shown in bright blue and are highlighted by blue arrows. Black arrows indicate the shift of the catalytic domain imposed by the presence of the C-terminal lock. Distances between representative corresponding atoms in the two structures are indicated. (*c*, *d*) Top and side views of the electrostatic potential surfaces of (*c*) Ldt_{Mt1} and (*d*) Ldt_{Mt2}. The greatest differences in the electrostatic potential surfaces close to the catalytic site are highlighted by black ellipses.

3.3. Comparisons with Ldt_{Mt2}

Recently, the structures of different variants of Ldt_{Mt2}, one of the homologues of Ldt_{Mt1} (37% sequence identity overall), have been reported (Böth *et al.*, 2013; Kim *et al.*, 2013; Erdemli *et al.*, 2012). Structural comparison shows an overall similarity of the two proteins (r.m.s.d. of 1.5 Å computed on C^{α} atoms), albeit with significant differences. Ldt_{Mt1} is a smaller homologue of Ldt_{Mt2}, as Ldt_{Mt2} contains an extra N-terminal domain and several insertions (Böth *et al.*, 2013).

A superposition of the catalytic domains of Ldt_{Mt1} and Ldt_{Mt2} shows strong conservation of the enzyme catalytic sites. Indeed, Cys226, His208 and Ser209 are conserved in Ldt_{Mt1} and present the same conformations as observed in the Ldt_{Mt2} structure

(Fig. 4). However, whereas Cys226 and His208 are conserved in all Mtb homologues of Ldt_{Mt1}, Ser209 is replaced by Ala in the Ldt_{Mt1} homologue MT0501 (data not shown). This finding is consistent with the observation of a hydrogen-bonding interaction between the His208 side chain and the backbone carbonyl O atom of the catalytic serine (Fig. 4). A conformational change characterizes the cap, which is shifted by about 2.5 Å in Ldt_{Mt1} compared with the structure of Ldt_{Mt2} in complex with a peptidoglycan fragment (Erdemli *et al.*, 2012). However, the cap is completely disordered in the apo structure of Ldt_{Mt2} crystallized in a different space group (Kim *et al.*, 2013). This finding suggests that these differences may be an effect of crystal packing and may reflect a high level of flexibility of the cap region.

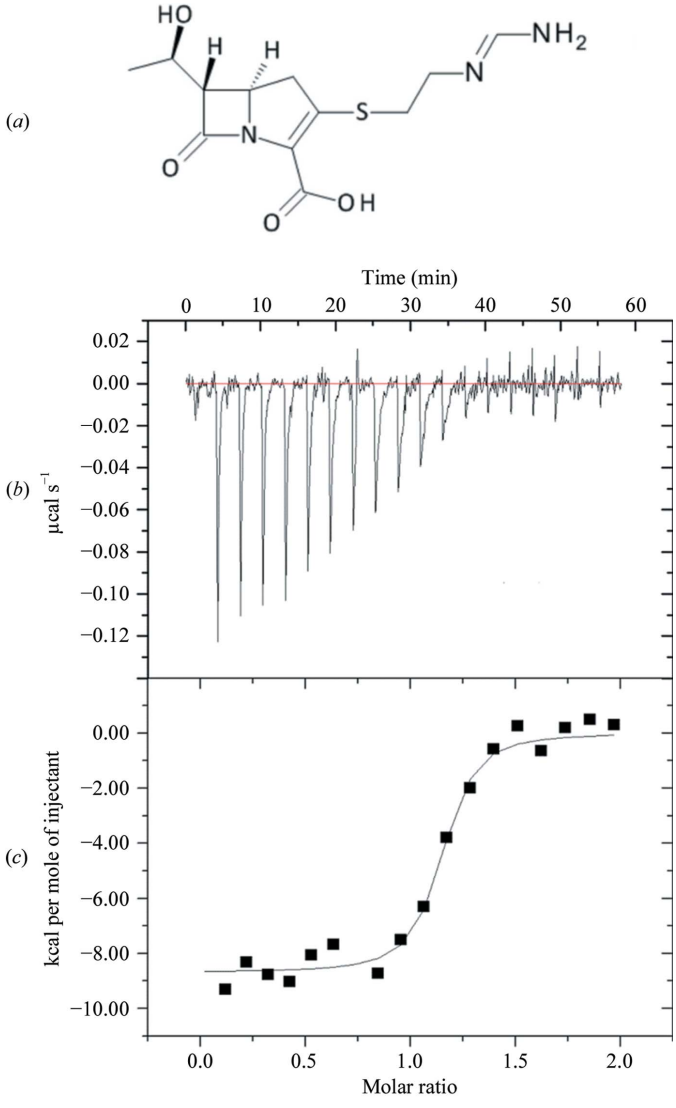

Figure 6
Isothermal titration calorimetry experiments. (*a*) The chemical structure of imipenem. (*b*) Raw data for the titration of Ldt_{Mt1} with imipenem at 298 K. (*c*) Integrated heats of binding obtained from the raw data after subtracting the heat of dilution. The solid line represents the best curve fit to the experimental data using the 'one-set-of-sites' model from MicroCal *Origin*.

Differences exist in the Ig-like domains of the two proteins. Despite overall conservation of the Ig-like fold (r.m.s.d. on C^{α} atoms of 1.0 Å), a long deletion exists between β-strands $\beta6$ and $\beta7$ of Ldt_{Mt1} compared with the equivalent domain in Ldt_{Mt2} (Figs. 5*a* and 5*b*). In Ldt_{Mt2} this region forms a two-stranded β-sheet with the N-terminal β-strand, which forms a lid over the Ig-like domain and interacts with α-helix $\alpha1$ through hydrophobic interactions (Figs. 5*a* and 5*b*). Most importantly, a substantial difference exists in the inter-domain orientation of the Ig-like and catalytic domains of the two homologues. After superposition of the Ig-like domains of the two proteins, the catalytic domain of Ldt_{Mt2} is significantly roto-translated, with a displacement of 6.1 Å for the catalytic Cys226 (Ldt_{Mt1} numbering) and a maximum displacement of 8.5 Å for more peripheral regions (Fig. 5*b*). The different domain orientation observed in the two homologues is likely to be a consequence of the C-terminal 29-residue extension in Ldt_{Mt2} (CTSD domain; Erdemli *et al.*, 2012) which connects the catalytic domain to the adjacent Ig-like domains and is absent in Ldt_{Mt1} (Figs. 5*a* and 5*b*). This moiety is likely to lock the relative orientation of the two domains in Ldt_{Mt2}, whereas the lower number of interactions that exist between the Ig-like and catalytic domains of Ldt_{Mt1} suggests a more flexible nature of this latter enzyme.

Although Ldt_{Mt1} and Ldt_{Mt2} share high sequence identity, they display completely different electrostatic potential surfaces, with a more negatively charged surface computed for Ldt_{Mt2} (Figs. 5*c* and 5*d*). Indeed, the most conserved residues constitute the protein core, whereas the surface residues vary significantly. The more negative electrostatic potential surface of Ldt_{Mt2} correlates well with the higher value of the calculated pI for Ldt_{Mt1} (pI of 7.4) compared with Ldt_{Mt2} (pI of 5.1 for the region equivalent to Ldt_{Mt1} and 6.0 overall). The functional impact of the distinctive structural features of Ldt_{Mt1} and Ldt_{Mt2} has not been investigated, but it is tempting to speculate that they may be associated with modulation of the L,D-transpeptidase function, substrate specificity/selectivity and/or interaction with other proteins.

3.4. Isothermal titration calorimetry

β-Lactams are generally considered to be effective inhibitors not because they bind tightly but because they are reactive acylating agents (Kluge & Petter, 2010). However, the presence of an enzyme–inhibitor complex was demonstrated for Ldt_{Mt1} before the irreversible acylation (Dubée, Triboulet *et al.*, 2012). Therefore, we measured the binding affinity of Ldt_{Mt1} for imipenem using isothermal titration calorimetry (ITC; Fig. 6). Binding isotherms for the interaction of Ldt_{Mt1} with imipenem measured at pH 6.0 were characterized by exothermic heats of binding which decreased in magnitude with successive injections until saturation was achieved (Fig. 6). The shape of the binding isotherm indicates the presence of an equilibrium between bound and unbound species (Fig. 6). Consistent with the several noncovalent interactions observed in the crystal structure of Ldt_{Mt1} in complex with imipenem, our data indicate strong enzyme–

inhibitor binding, with K_d and ΔH values of 62.1 (±11.2) nM and 36.4 (±0.8) kJ mol^{-1}, respectively. These values are in close agreement with those reported for the binding of imipenem to Ldt_{Mt2} (Erdemli *et al.*, 2012).

3.5. Crystal structure of Ldt_{Mt1} bound to the β-lactam imipenem

The finding that β-lactams are able to eradicate XDR-TB if the bacterial β-lactamase BlaC is inactivated has prompted recent research on the potential use of β-lactams in therapy (Hugonnet *et al.*, 2009). Understanding the interactions of β-lactams with L,D-transpeptidases may facilitate the development of improved antibacterial strategies. Mass-spectrometric and kinetic analyses have previously shown that carbapenems bind covalently to Ldt_{Mt1} and Ldt_{Mt2} of Mtb. These data showed that the carbapenems meropenem, doripenem, imipenem and ertapenem covalently bind Ldt_{Mt1} with fast kinetics, with ertapenem and imipenem being the most efficient drugs for *in vitro* Ldt_{Mt1} inactivation (Dubée, Triboulet *et al.*, 2012).

To provide a detailed structural view of how imipenem inhibits Ldt_{Mt1}, we have determined the crystal structure of Ldt_{Mt1} in complex with imipenem. Electron-density maps clearly showed contiguous density with the S^{γ} atom of the catalytic Cys226 (Fig. 7*a*). This finding confirms that inactivation of Ldt_{Mt1} occurs through enzyme acylation generated by the opening of the β-lactam ring and the formation of a thioester bond (Dubée, Triboulet *et al.*, 2012). This study provides the first detailed structural view of the interactions between imipenem and Ldt_{Mt1} (Fig. 7), thus setting up a basis for the design of improved anti-TB carbapenems. Imipenem sits in the centre of the catalytic tunnel of Ldt_{Mt1}, with its C7 carbonyl atom covalently bonded to Cys226 and its O7 carbonyl O atom forming hydrogen bonds to the backbone N atoms of both Cys226 and Gly225 (Fig. 7*b*). Two moieties are key to the anchoring and the orientation of imipenem in the enzyme tunnel: the C2 carboxyl and the C8 hydroxyl groups, which point towards the two opposite entrances of the tunnel (Fig. 7*c*). The C8 hydroxyl group forms a hydrogen bond to the carbonyl O atom of Gly225, whereas the C2 carboxyl group is hydrogen-bonded to both the main chain and the side chain of His224 and to the side chains of His208 and Asn228 (Fig. 7). In addition, the pyrroline ring of imipenem is stabilized by Tyr190 through hydrophobic interactions. All of these residues are highly conserved among L,D-transpeptidase homologues (Supplementary Fig. S2). No electron density was detectable beyond the thioether S atom for the R3 chain of imipenem, indicating a high conformational freedom for this chain (Fig. 7*a*).

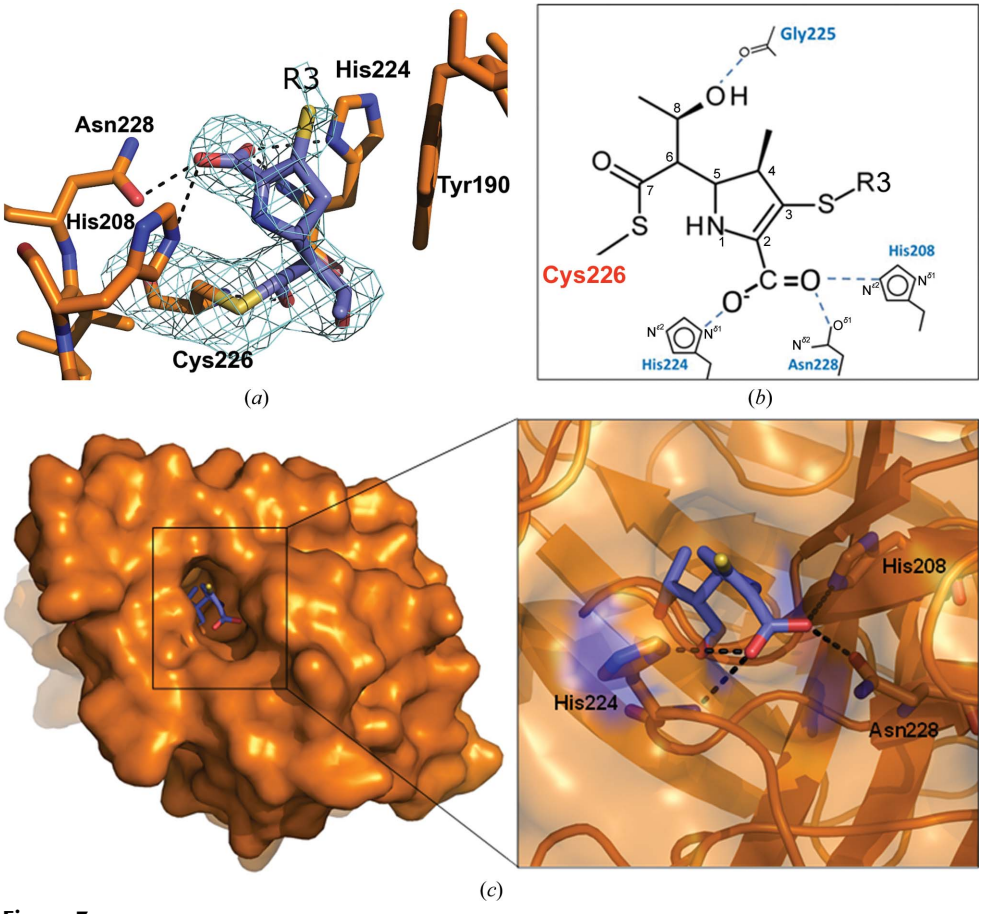

Figure 7
Crystal structure of imipenem-inactivated Ldt_{Mt1}. (*a*) OMIT ($F_o - F_c$) electron-density map contoured at 3σ for imipenem; interacting residues are shown in stick representation. (*b*) Sketch of interactions between Ldt_{Mt1} and imipenem. The R3 chain is not visible in the electron-density maps. (*c*) A bound imipenem molecule in the active-site tunnel; the inset shows the main interactions involving the carboxyl group of the drug.

Complexes between L,D-transpeptidases and β-lactams have recently been reported (Kim *et al.*, 2013; Lecoq *et al.*, 2012, 2013). Binding of the β-lactam meropenem to Ldt_{Mt2} was shown to induce a conformational change of the active-site lid (Kim *et al.*, 2013). Namely, the lid was observed to be disordered in the crystal structure of the apo form and to move close to the active-site pocket when Ldt_{Mt2} binds to meropenem. In the structure of the imipenem complex of Ldt_{Mt1}, we only observed tiny conformational changes compared with the apo structure, such as the reorientation of His208 to form a hydrogen bond to the carboxyl group of the drug (Supplementary Fig. S4). This finding is likely to be owing to the fact that the

active-site lid is already well structured and in a closed conformation in the structure of the Ldt_{Mt1} apo form.

A comparison of the binding mode of imipenem to Ldt_{Mt1} with that of meropenem to Ldt_{Mt2} shows that the two β-lactams exhibit different orientations (Kim *et al.*, 2013; Supplementary Fig. S5). A further conformation is adopted by the β-lactam ertapenem when in complex with the L,D-transpeptidase from *E. faecium* (Lecoq *et al.*, 2013; Supplementary Fig. S5). On the other hand, the structure of L,D-transpeptidase from *B. subtilis* in complex with imipenem shows that this β-lactam adopts a wide conformational ensemble (Lecoq *et al.*, 2012). High flexibility is also observed for the catalytic cysteine, indicating the absence of preferential orientations of the drug. As previously suggested, it is likely that the specificity of β-lactams for L,D-transpeptidases is not determined by enthalpically favourable drug–protein interactions but is merely determined by the chemical step of the reaction, probably at the activation step of the catalytic cysteine. These findings indicate that β-lactams are amenable to modifications in order to improve their interactions with their target. Consistently, it has been shown that different side chains of carbapenems modulate drug-binding and acylation rates (Dubée, Triboulet *et al.*, 2012).

4. Conclusions

Ldt_{Mt1} is upregulated 17-fold during the stationary phase and is thought to play a role in bacterial adaptation to the dormant state (Betts *et al.*, 2002). Thus, Ldt_{Mt1} could be an essential target that accounts for the bactericidal activity of carbapenem–clavulanic acid against dormant forms of Mtb. In this work, we determined the crystal structures of Ldt_{Mt1} in its free state and in complex with the β-lactam imipenem.

The crystal structure shows that the catalytic site of Ldt_{Mt1} is located in a tiny tunnel, a finding which accounts well for the typically high specificity, as observed in *E. faecium*, of this class of enzymes towards PGN precursors (Magnet *et al.*, 2007). Computation of the pK_a values of the catalytic residues based on the crystal structure of Ldt_{Mt1} shows that Cys226 remains protonated at neutral pH (pK_a = 11.1), whereas His208 is positively charged (pK_a = 4.6). Therefore, the crystal structure of Ldt_{Mt1} suggests that His208 is likely to act as a general base to activate Cys226 for nucleophilic attack. In addition, we provide analogies and differences between Ldt_{Mt1} and its homologue Ldt_{Mt2}; these structural features are likely to form the basis of the different functional roles of the two enzymes.

In the crystal structure of Ldt_{Mt1} complexed with imipenem the catalytic tunnel is nearly completely occupied by the β-lactam. Apart from the catalytic His208 and Cys226, which covalently bind the drug, another two residues are important for imipenem binding. These are His224 and Asn228; both residues, together with His208, anchor the carboxyl group of imipenem (Fig. 7). Part of the bound imipenem molecule, namely the R3 side chain, is not structured. This feature makes β-lactams amenable to modifications to enhance their interactions with their target. The structural information obtained on Ldt_{Mt1} may be key to the development of improved inhibitors.

This work was funded by the Ministero Italiano dell' Istruzione, dell'Università e della Ricerca (PRIN 2009 – prot. 200993WWF9) and by the Mizutani Foundation of Glycoscience (Reference No. 120012). The authors also acknowledge the COST Action BM1003 (COST-Grants-BM1003-00772).

References

Berisio, R., Ciccarelli, L., Squeglia, F., De Simone, A. & Vitagliano, L. (2012). *Protein Pept. Lett.* **19**, 1045–1053.
Betts, J. C., Lukey, P. T., Robb, L. C., McAdam, R. A. & Duncan, K. (2002). *Mol. Microbiol.* **43**, 717–731.
Biarrotte-Sorin, S., Hugonnet, J.-E., Delfosse, V., Mainardi, J.-L., Gutmann, L., Arthur, M. & Mayer, C. (2006). *J. Mol. Biol.* **359**, 533–538.
Böth, D., Steiner, E. M., Stadler, D., Lindqvist, Y., Schnell, R. & Schneider, G. (2013). *Acta Cryst.* D**69**, 432–441.
Chim, N. *et al.* (2011). *Tuberculosis*, **91**, 155–172.
Correale, S., Ruggiero, A., Pedone, E. & Berisio, R. (2013). *Acta Cryst.* F**69**, 253–256.
Dubée, V., Arthur, M., Fief, H., Triboulet, S., Mainardi, J.-L., Gutmann, L., Sollogoub, M., Rice, L. B., Ethève-Quelquejeu, M. & Hugonnet, J.-E. (2012). *Antimicrob. Agents Chemother.* **56**, 3409–3412.
Dubée, V., Triboulet, S., Mainardi, J.-L., Ethève-Quelquejeu, M., Gutmann, L., Marie, A., Dubost, L., Hugonnet, J.-E. & Arthur, M. (2012). *Antimicrob. Agents Chemother.* **56**, 4189–4195.
Dworkin, J. & Shah, I. M. (2010). *Nature Rev. Microbiol.* **8**, 890–896.
England, K., Boshoff, H. I., Arora, K., Weiner, D., Dayao, E., Schimel, D., Via, L. E. & Barry, C. E. III (2012). *Antimicrob. Agents Chemother.* **56**, 3384–3387.
Erdemli, S. B., Gupta, R., Bishai, W. R., Lamichhane, G., Amzel, L. M. & Bianchet, M. A. (2012). *Structure*, **20**, 2103–2115.
Finn, R. D., Mistry, J., Schuster-Böckler, B., Griffiths-Jones, S., Hollich, V., Lassmann, T., Moxon, S., Marshall, M., Khanna, A., Durbin, R., Eddy, S. R., Sonnhammer, E. L. & Bateman, A. (2006). *Nucleic Acids Res.* **34**, D247–D251.
Goldenberg, O., Erez, E., Nimrod, G. & Ben-Tal, N. (2009). *Nucleic Acids Res.* **37**, D323–D327.
Gul, S., Hussain, S., Thomas, M. P., Resmini, M., Verma, C. S., Thomas, E. W. & Brocklehurst, K. (2008). *Biochemistry*, **47**, 2025–2035.
Gupta, R., Lavollay, M., Mainardi, J.-L., Arthur, M., Bishai, W. R. & Lamichhane, G. (2010). *Nature Med.* **16**, 466–469.
Hugonnet, J.-E. & Blanchard, J. S. (2007). *Biochemistry*, **46**, 11998–12004.
Hugonnet, J.-E., Tremblay, L. W., Boshoff, H. I., Barry, C. E. III & Blanchard, J. S. (2009). *Science*, **323**, 1215–1218.
Kaprelyants, A. S., Mukamolova, G. V., Ruggiero, A., Makarov, V. A., Demina, G. R., Shleeva, M. O., Potapov, V. D. & Shramko, P. A. (2012). *Protein Pept. Lett.* **19**, 1026–1034.
Kim, H. S., Kim, J., Im, H. N., Yoon, J. Y., An, D. R., Yoon, H. J., Kim, J. Y., Min, H. K., Kim, S.-J., Lee, J. Y., Han, B. W. & Suh, S. W. (2013). *Acta Cryst.* D**69**, 420–431.
Kluge, A. F. & Petter, R. C. (2010). *Curr. Opin. Chem. Biol.* **14**, 421–427.
Langer, G., Cohen, S. X., Lamzin, V. S. & Perrakis, A. (2008). *Nature Protoc.* **3**, 1171–1179.
Laskowski, R. A., Rullmann, J. A. C., MacArthur, M. W., Kaptein, R. & Thornton, J. M. (1996). *J. Biomol. NMR*, **8**, 477–486.
Lavollay, M., Arthur, M., Fourgeaud, M., Dubost, L., Marie, A., Veziris, N., Blanot, D., Gutmann, L. & Mainardi, J.-L. (2008). *J. Bacteriol.* **190**, 4360–4366.

Lecoq, L., Bougault, C., Hugonnet, J.-E., Veckerlé, C., Pessey, O., Arthur, M. & Simorre, J.-P. (2012). *Structure*, **20**, 850–861.
Lecoq, L., Dubée, V., Triboulet, S., Bougault, C., Hugonnet, J.-E., Arthur, M. & Simorre, J.-P. (2013). *ACS Chem. Biol.*, doi:10.1021/cb4001603.
Magnet, S., Arbeloa, A., Mainardi, J.-L., Hugonnet, J.-E., Fourgeaud, M., Dubost, L., Marie, A., Delfosse, V., Mayer, C., Rice, L. B. & Arthur, M. (2007). *J. Biol. Chem.* **282**, 13151–13159.
Mainardi, J.-L., Fourgeaud, M., Hugonnet, J.-E., Dubost, L., Brouard, J.-P., Ouazzani, J., Rice, L. B., Gutmann, L. & Arthur, M. (2005). *J. Biol. Chem.* **280**, 38146–38152.
Mainardi, J.-L., Hugonnet, J.-E., Rusconi, F., Fourgeaud, M., Dubost, L., Moumi, A. N., Delfosse, V., Mayer, C., Gutmann, L., Rice, L. B. & Arthur, M. (2007). *J. Biol. Chem.* **282**, 30414–30422.
Mukamolova, G. V., Kaprelyants, A. S., Young, D. I., Young, M. & Kell, D. B. (1998). *Proc. Natl Acad. Sci. USA*, **95**, 8916–8921.
Mukamolova, G. V., Yanopolskaya, N. D., Kell, D. B. & Kaprelyants, A. S. (1998). *Antonie Van Leeuwenhoek*, **73**, 237–243.
Murillo, A. C. *et al.* (2007). *Infect. Disord. Drug Targets*, **7**, 127–139.
Otwinowski, Z. & Minor, W. (1997). *Methods Enzymol.* **276**, 307–326.
Rostkowski, M., Olsson, M. H., Søndergaard, C. R. & Jensen, J. H. (2011). *BMC Struct. Biol.* **11**, 6.
Ruggiero, A., De Simone, P., Smaldone, G., Squeglia, F. & Berisio, R. (2012). *Curr. Protein Pept. Sci.* **13**, 756–766.
Ruggiero, A., Marasco, D., Squeglia, F., Soldini, S., Pedone, E., Pedone, C. & Berisio, R. (2010). *Structure*, **18**, 1184–1190.
Ruggiero, A., Marchant, J., Squeglia, F., Makarov, V., De Simone, A. & Berisio, R. (2013). *J. Biomol. Struct. Dyn.* **31**, 195–205.
Ruggiero, A., Squeglia, F., Marasco, D., Marchetti, R., Molinaro, A. & Berisio, R. (2011). *Biochem. J.* **435**, 33–41.
Ruggiero, A., Tizzano, B., Pedone, E., Pedone, C., Wilmanns, M. & Berisio, R. (2009). *J. Mol. Biol.* **385**, 153–162.
Squeglia, F., Marchetti, R., Ruggiero, A., Lanzetta, R., Marasco, D., Dworkin, J., Petoukhov, M., Molinaro, A., Berisio, R. & Silipo, A. (2011). *J. Am. Chem. Soc.*, **133**, 20676–20679.
Terwilliger, T. (2004). *J. Synchrotron Rad.* **11**, 49–52.
Trefzer, C., Škovierová, H., Buroni, S., Bobovská, A., Nenci, S., Molteni, E., Pojer, F., Pasca, M. R., Makarov, V., Cole, S. T., Riccardi, G., Mikušová, K. & Johnsson, K. (2012). *J. Am. Chem. Soc.* **134**, 912–915.
Winn, M. D. *et al.* (2011). *Acta Cryst.* D**67**, 235–242.